Received: 11 June 2024 | Revised: 6 September 2024 | Accepted: 3 October 2024

DOI: 10.1111/jace.20217

Journal of the American Ceramic Society

RESEARCH ARTICLE

Modeling of ternary ion exchange and stress evolution in lithium-containing glass

Junju Xu[1,2] | **Yuzhou Zhang**[1] | **Yajing Zhang**[3] | **Chen Lin**[3] | **Ziyang Gao**[2] | **Haihui Ruan**[1]

[1]Department of Mechanical Engineering, The Hong Kong Polytechnic University, Hong Kong, China

[2]Hong Kong Applied Science and Technology Research Institute, Hong Kong Science Park, Shatin, Hong Kong

[3]Sino-French Institute of Nuclear Engineering and Technology, Sun Yat-Sen University, Zhuhai, China

Correspondence

Haihui Ruan, Department of Mechanical Engineering, The Hong Kong Polytechnic University, Hong Kong 999077, China.
Email: haihui.ruan@polyu.edu.hk

Chen Lin, Sino-French Institute of Nuclear Engineering and Technology, Sun Yat-Sen University, Zhuhai 519080, China.
Email: linch67@mail.sysu.edu.cn

Funding information

Hong Kong GRF, Grant/Award Number: 15210622; HKPolyU, Grant/Award Number: P0039303; The Hong Kong Branch of National Engineering Research Centre for Application Specific Integrated Circuit System (CNERC); Hetao Shenzhen-Hong Kong Science and Technology Innovation Cooperation Zone Project, Grant/Award Number: HTHZQSWS-KCCYB-2023042; Natural Science Foundation of Guangdong Province, Grant/Award Numbers: 2022A1515011891, 2024A1515011127; Natural Science Basic Research Plan in Shaanxi Province, Grant/Award Number: 2022JQ-019; Young Top Talents; Pearl River Talent Project of Guangdong Province, Grant/Award Number: 2021QN02L344

Abstract

A computational model of ternary ion exchange (IOX) for strengthening glass is proposed to predict the cation concentration and residual stress distributions in glass after ternary IOX. The comparison between theoretical predictions and experimental results indicated the validates the model. Additionally, it provides a method to determine ion diffusivity and volume expansion through ternary IOX experiments. Simulations of K–Na–Li ternary IOX were conducted using the parameters calibrated based on experimental results from a thick silicate glass. Then the process parameters were changed to clarify their influences. Key findings reveal that for thick glass (where lateral expansion is negligible), the optimum ratio of K^+ and Na^+ concentrations in a molten salt is 2:1. We further consolidate the effects of process parameters by training a neural network (NN) and demonstrate that the NN can be a surrogate model to replace the time-consuming simulations, which could be more adaptable by the glass industry.

KEYWORDS

glass, ion exchange, mechano-electrochemical modeling, neural network

Junju Xu and Yuzhou Zhang contributed equally to this study.

1 | INTRODUCTION

Glass has an extremely wide range of applications[1,2] due to its chemical inertness and optical transparency. However, it is prone to cracking during usage.[3] Theoretically, the strength of a defect-free oxide glass specimen can reach up to 10 GPa, but in practice, the actual strength of glass is significantly lower.[4] In 1962, Kistler[5] and Acloque[6] proposed the ion exchange (IOX) method to strengthen thin glass sheets, which has since been widely adopted in glass manufacturing, especially for strengthening glass covers for electronic products. The IOX process refers to the diffusive exchange of cations between glass and molten salts, resulting in changes to the mechanical and optical properties of the layers with altered composition. Typically, the volume of the cations in molten salts is usually larger than that of the exchanging counterparts, leading to large compressive stresses in the surface layers of glass workpieces, which reduces the tendency of cracking caused by surface flaws. Due to increased strength and surface hardness, chemically strengthened glass is suitable for the manufacturing of thin (thickness ≤ 1 mm) and ultrathin (thickness ≤ 0.1 mm) cover glass.[7–9]

Several ion pairs are used in IOX, such as Ag–Na[10] and Cs–Na,[11] and the most commonly used one is the exchange of K^+ in molten salt for Na^+ in glass workpieces.[12] However, the strengthening effect in such a binary system is limited, as the depth of layer (DOL) generated by IOX is generally well below 100 μm.[13] Prolonging IOX time to achieve a larger DOL can compromise surface compressive stress (SCS) due to stress relaxation.[14] Therefore, ternary IOX systems have been introduced; with K–Na–Li IOX becoming particularly prevalent in the cover glass industry.[15–22] Because lithium-ion has a small size and high diffusivity, ternary IOX can be performed at temperatures lower than that of the binary K–Na IOX to achieve an even higher SCS and DOL. For example, Jiang et al.[8] examined the chemical strengthening of Li^+-containing phosphosilicate glass and found that, compared with a binary K-Na IOX process, a two-step ternary K–Na–Li IOX ternary treatment increased the DOL by 160% and the Vicker hardness by 18.5% (due to the increase in SCS).

With the successful application of ternary IOX in thin glass products, a critical problem is to propose a computational model describing the mechano-electrochemical process to predict the strengthening effect and assist in the parametric design of an IOX process. In the glass manufacturing industry, the optical waveguide method is employed to measure SCS and DOL of chemically strengthened glass workpieces.[23] It is a nondestructive measurement method with high precision and simple operation; however, it relies on the ad hoc assumption of residual stress field, often lacking a clear physical ground (for example, in the patent,[21] a quadric stress profile was presumed). Concerning this issue, a computational model for ternary IOX, predicting the residual stress distribution, is needed.[24–26]

The computational study of IOX is currently insufficient in the literature. Inman[27] and Lupascu[28] extended Fick's law to incorporate nonideal cation behavior (i.e., concentration-dependent self-diffusion coefficients) to address the observed mixed ion effects.[29,30] However, their model did not consider the impact of stress on diffusivity. Macrelli et al.[31] proposed a numerical model for binary IOX to investigate the coupling between stress and diffusion, as demonstrated by previous experimental studies.[32–34] This model is one-dimensional with the simplifications that the glass is purely elastic and charge neutrality is enforced. Lin et al.[35] later introduced a mechano-electrochemical coupling model under the large-strain and viscoelastic framework to describe the deformation of thin glass after IOX, which leads to stress relief. Their model included the formulations describing the mechano-electrochemical coupling in IOX but still limited to binary systems.

Although the computational models for IOX, that is, the numerical solutions of the equations governing ion transports and stress buildup, can predict SCS and DOL of glass after an IOX process, such numerical processes are still very time-consuming. A surrogate model replacing the tedious numerical solutions could be more beneficial for the industry. Such a model can be established based on machine learning (ML) approaches that leverage existing datasets to infer data-driven models.[36] These methods have proven to be effective in various engineering problems, such as materials development,[36] structural design,[37,38] and manufacturing.[39,37] In glass research, Cassar[38] proposed a neural network (NN) model to predict the fragility of oxide glass-forming liquids based on their compositions and temperature-dependent viscosity. This model has demonstrated exceptional predictive performance and can assist in selecting compositions with desired properties for specific applications.

To the best of our knowledge, a numerical model has not been available to describe ternary IOX, despite its widespread use in the industry. Therefore, we develop a new computational model of ternary IOX based on our previous work[35] that incorporated the large deformation theory (because the eigenstrains associated with IOX are not small) and a viscoelastic constitutive relation (because the stress relaxation is nonnegligible, especially for SCS). For a ternary IOX, such as the K–Na–Li system, we simplified it to be K–Na and Na–Li exchanges, assuming that direct K–Li exchange is unlikely to occur.[40] Through parametric studies and comparison with experimental results, we discussed the effects of ion concentration on diffusivity and

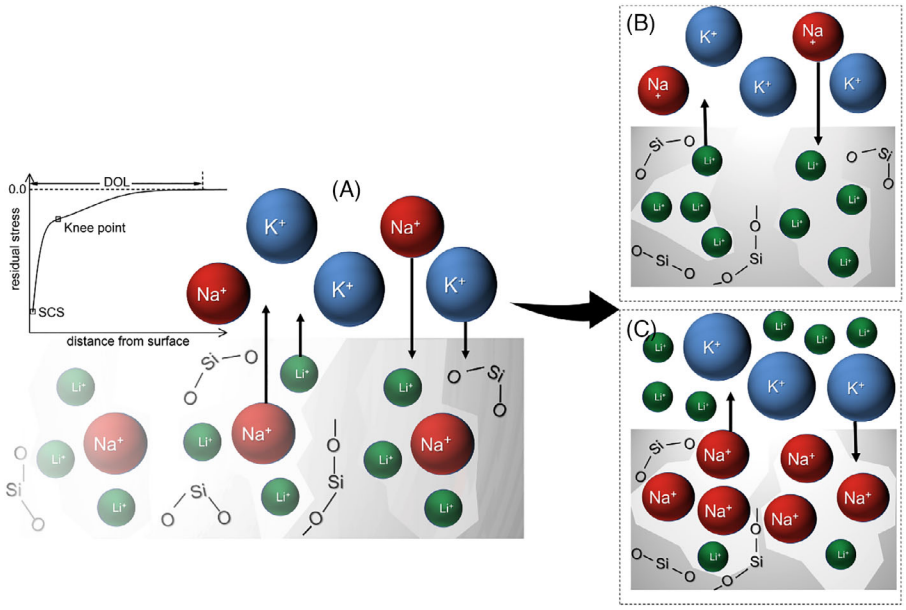

FIGURE 1 Schematic diagram of the formation of ternary IOX compressive stress layer for K–Na–Li system in the lithium–silicate glass. IOX, ion exchange.

molten salt composition on SCS and DOL. These numerical studies generate extensive data, enabling us to establish an NN model to assist in predicting SCS and DOL from the input of IOX process parameters and glass thickness.

2 | METHODS

The schematic of a ternary IOX involving K^+, Na^+, and Li^+ ions is shown in Figure 1A. This mechanochemical process is divided into two exchange processes as shown in Figure 1B,C. We assume that when a lithium-containing glass is immersed in a molten salt electrolyte containing Na^+ and K^+, Na^+ ions in the molten salt first exchange with Li^+ in the glass, represented by the reaction: Na^+ (salt) + Li^+ (glass) → Li^+ (salt) + Na^+ (glass). This results in the formation of sodium-containing surface layers of the glass (as illustrated in Figure 1B). While the Li-Na exchange continues, K^+ in the molten salt exchanges with Na^+ in the glass, described by the reaction: K^+(salt) + Na^+ (glass) → Na^+ (salt) + K^+ (glass) (i.e., Figure 1C). The exchange of ions leads to a local expansion in glass, creating compressive surface layers and corresponding tensile stresses in internal layers without IOX.

2.1 | Diffusion equation for ternary IOX

Denoting by subscript i a kind of ions in exchange and adopting the Nernst–Planck law, the ion flux, $\mathbf{j}_i$, is given by Equation (1):

$$\mathbf{j}_i = \mu_i c_i \mathbf{E} - D_i \nabla c_i , \tag{1}$$

where $\mathbf{E}$ is an electric field caused by the transient charge distribution and an externally applied field, D_i is the diffusion coefficient, and μ_i is the ion mobility. With the Fick's second law, the variation of concentration c_i is expressed as Equation (2):

$$\frac{\partial c_i}{\partial t} = -\nabla \mathbf{j}_i = -\mu_i \nabla c_i \cdot \mathbf{E} - \mu_i c_i \nabla \mathbf{E} + D_i \nabla^2 c_i . \tag{2}$$

According to the molecular dynamics analysis by Olmsted et al.,[41] diffusion must overcome an energy barrier resulting from the interaction with neighboring atoms, which is closely related to stresses. Therefore, stress-dependent diffusivity is assumed, which is expressed as Equation (3):

$$D_i = D_{i,sf} \exp\left(-\frac{(Q_b(\boldsymbol{\sigma}))}{RT}\right), \tag{3}$$

where $D_{i,sf}$ is the stress-free diffusion coefficient, and $Q_b(\sigma)$ is the stress-dependent activation energy, expressed as $Q_b(\sigma) = -\xi \mathrm{tr}(\boldsymbol{\sigma})$[42] with $\mathrm{tr}(\boldsymbol{\sigma})$ and ξ being the trace of the stress tensor $\boldsymbol{\sigma}$ and activation volume, respectively.

It is assumed that the total ion flux, $\mathbf{j_0}$ (Equation 4)

$$\sum_i^N \mathbf{j}_i = \mathbf{j}_0 , \tag{4}$$

is zero because no external field that generates a net current is applied. With the assumption of space charge neutrality, we have Equation (5):

$$\sum_{\mathrm{i}}^{\mathrm{N}} c_{\mathrm{i}} = c_0 \,, \tag{5}$$

where c_0 is a constant equal to the initial concentration of the concerned ions, for K–Na–Li IOX, c_0 is the concentration of lithium and sodium in the original glass.

Substituting Equation (1) into Equation (4) gives Equation (6):

$$\sum_{\mathrm{i}}^{\mathrm{N}} \mu_{\mathrm{i}} c_{\mathrm{i}} \mathbf{E} - D_{\mathrm{i}} \nabla c_{\mathrm{i}} = \mathbf{j}_0 \,. \tag{6}$$

It can be deduced that

$$\mathbf{E} = \frac{\mathbf{j}_0 + \sum_i^{N-1} (D_i - D_N) \nabla c_i}{\sum_i^{N-1} (\mu_i - \mu_N) c_i + \mu_N c_0} \,, \tag{7}$$

$$\nabla \boldsymbol{E} = \frac{\nabla j_0 + \left(\sum_i^{N-1} (D_i - D_N) \nabla^2 c_i\right) - \left(\sum_i^{N-1} (\mu_i - \mu_N) \nabla c_i\right) \cdot \boldsymbol{E}}{\sum_i^{N-1} (\mu_i - \mu_N) c_i + \mu_N c_0} \,. \tag{8}$$

Defining $\bar{c}_i = \frac{c_i}{c_0}$ and substituting Equations (7) and (8) into Equation (2), the governing equation of diffusion can finally be recast as Equation (9):

$$\frac{\partial \bar{c}_i}{\partial t} = D_i \nabla^2 \bar{c}_i - \frac{\mu_i \bar{c}_i \left(\nabla j_0 + \sum_i^{N-1} \left[(D_i - D_N) \nabla^2 \bar{c}_i\right]\right)}{\sum_i^{N-1} \left[(\mu_i - \mu_N) \bar{c}_i\right] + \mu_N} + \left(\frac{\mu_i \bar{c}_i \left(\sum_i^{N-1} \left[(\mu_i - \mu_N) \nabla \bar{c}_i\right]\right)}{\sum_i^{N-1} \left[(\mu_i - \mu_N) \bar{c}_i\right] + \mu_N} - \mu_i \nabla \bar{c}_i\right) \cdot \left(\frac{\sum_i^{N-1} \left[(D_i - D_N) \nabla \bar{c}_i\right]}{\sum_i^{N-1} \left[(\mu_i - \mu_N) \bar{c}_i\right] + \mu_N} + \nabla \varphi_{apply}\right), \tag{9}$$

where we specify

$$\frac{\mathrm{j}_0}{\sum_{\mathrm{i}}^{\mathrm{N}-1} \left[(\mu_{\mathrm{i}} - \mu_{\mathrm{N}}) \bar{c}_{\mathrm{i}}\right] + \mu_{\mathrm{N}}} = \nabla \varphi_{\mathrm{apply}} . \tag{10}$$

This term can be determined by solving the Poisson's equation (Equation 11):

$$\nabla^2 \varphi_{\mathrm{apply}} = 0. \tag{11}$$

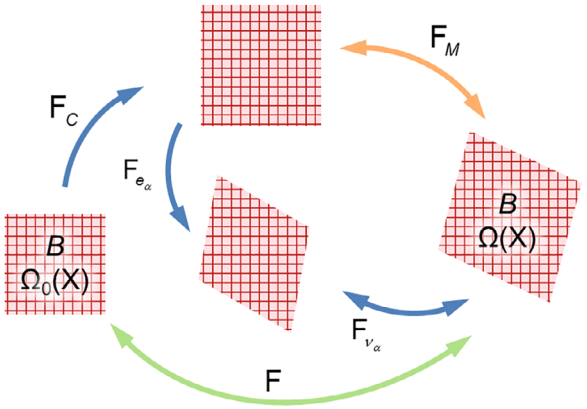

FIGURE 2 Schematics of the reference and deformed configurations, denoted by Ω_0 and Ω, respectively, of which the total deformation gradient tensor $\mathbf{F}$ is decomposed multiplicatively into compositional transformation $\mathbf{F}_c$, elastic, $\mathbf{F}_{e_\alpha}$, and viscous, $\mathbf{F}_{v_\alpha}$, parts.

In a K–Na–Li ternary IOX, the reaction generally starts with the Na–Li exchange. When the concentration of Na^+ in the glass is greater than zero, K–Na exchange can occur. Our model describes such a stepwise IOX based on Equations (9–11).

2.2 | Constitutive relation considering large viscoelastic deformation behavior

Ion exchange leads to deformation and stress development. Owing to the significant change in molar volume during Na–Li and K–Na exchanges, the deformation of glass is modeled in a finite strain framework. As shown in Figure 2, let B denote a solid occupying a region Ω_0 in space with a fixed reference configuration. We define the geometric variation of B in terms of the smooth function $\mathbf{u}(\mathbf{X}) = \mathbf{x}(\mathbf{X}) - \mathbf{X}$, where the function maps each point in B, with coordinate $\mathbf{X}$, to a new point, with coordinate $\mathbf{x}$. Denoting by $\boldsymbol{I}$ the second-order identity tensor, and $\nabla_{\mathbf{X}}$ the gradient operator with respect to $\mathbf{X}$, the gradient of deformation at any point in B is $\mathbf{F} = \partial \mathbf{x}/\partial \mathbf{X} = \boldsymbol{I} + \nabla_{\mathbf{X}} \mathrm{u}$.

The multiplicative decomposition of the deformation gradient $\mathbf{F}$ (as shown in Figure 2) is (Equation 12):

$$\mathbf{F} = \mathbf{F}_M \, \mathbf{F}_C, \tag{12}$$

where $\mathbf{F}_M$ is the deformation gradient caused by mechanical deformation and $\mathbf{F}_C$ is the deformation gradient caused by composition changes during IOX. Assuming that the composition change only leads to a volumetric change

during IOX, $\mathbf{F}_C$ can be expressed as Equation (13):

$$\mathbf{F}_C = \left(1 + \frac{V_0 - V_1}{V_1}\bar{c}_{A^+}\right)^{\frac{1}{3}} \mathbf{I} = (J_C)^{\frac{1}{3}} \mathbf{I} = \mathbf{F}_C^{K-Na}\mathbf{F}_C^{Na-Li}, \tag{13}$$

where V_0 and V_1 are the molar volumes for the material with initial composition and the ion-exchanged composition, respectively; $\bar{c}_{A^+} = c_{A^+}/c_{B+}$ is the dimensionless concentration of ion A^+ with c_{B+} represents the initial concentration of host ions B^+; $J_C = 1 + (V_0 - V_1)\bar{c}_{A^+}/V_1$ represent the change in volume due to IOX.

For Na–Li IOX (Equation 14):

$$\mathbf{F}_C^{\mathrm{Na-Li}} = \left(1 + \frac{V_{\mathrm{SCG}} - V_{\mathrm{LCG}}}{V_{\mathrm{LCG}}}\bar{c}_{\mathrm{Na}^+}\right)^{\frac{1}{3}} \mathbf{I} = \left(J_C^{\mathrm{Na-Li}}\right)^{\frac{1}{3}} \mathbf{I}. \tag{14}$$

For K–Na IOX (Equation 15):

$$\mathbf{F}_C^{\mathrm{K-Na}} = \left(1 + \frac{V_{\mathrm{PCG}} - V_{\mathrm{SCG}}}{V_{\mathrm{SCG}}}\bar{c}_{K^+}\right)^{\frac{1}{3}} \mathbf{I} = \left(J_C^{\mathrm{K-Na}}\right)^{\frac{1}{3}} \mathbf{I}, \tag{15}$$

where V_{SCG}, V_{LCG}, and V_{PCG} are the molar volumes of the sodium-containing glass, lithium-containing glass, and potassium-containing glass, respectively.

The mechanical part of the deformation gradient, $\mathbf{F}_M$, can be further decomposed into the elastic and viscous components, as shown in Figure 2, which is given by Equation (16):

$$\mathbf{F}_M = \mathbf{F}_{e_\alpha}\,\mathbf{F}_{\upsilon_\alpha}, \tag{16}$$

where α represents the index of a Maxwell unit.

According to Neto et al.,[40] the relationship between the Cauchy stress tensor and the deformation gradient can be expressed as Equation (17):

$$\boldsymbol{\sigma} = \det(\mathbf{F})^{-1}\mathbf{P}\mathbf{F}^{\mathrm{T}}, \tag{17}$$

where $\mathbf{P}$ is the first Piola-Kirchhoff stress tensor. Following Lin et al.,[32] $\mathbf{P}$, can be expressed as $\mathbf{P} = \mathbf{P}_\infty + \sum_\alpha \mathbf{P}_\alpha$, where $\mathbf{P}_\infty$ and $\mathbf{P}_\alpha$ are the parts of the stress tensor, $\mathbf{P}$, accounting for the elastic contribution in the long-term equilibrium and the contribution from a Maxwell viscoelastic element, α, respectively. Based on the thermodynamic inequality, the expression of $\mathbf{P}_\infty$ and $\mathbf{P}_\alpha$ can be derived as (the detailed derivation can be seen in Supporting Information) Equations (18) and (19):

$$\mathbf{P}_\infty = \frac{\partial \Psi_\infty^{\mathrm{mech}}}{\partial \mathbf{F}_M}\,\mathbf{F}_C^{-\mathrm{T}} = \mathbf{F}_M\,\frac{\partial \Psi_\infty^{\mathrm{mech}}}{\partial \mathbf{E}_M}\mathbf{F}_C^{-\mathrm{T}}, \tag{18}$$

$$\mathbf{P}_\alpha = \frac{\partial \Psi_\alpha^{\mathrm{mech}}}{\partial \boldsymbol{F}_{e_a}}\,\mathbf{F}_{\upsilon_a}^{-T}\,\mathbf{F}_C^{-T} = \mathbf{F}_{e_a}\,\frac{\partial \Psi_\alpha^{\mathrm{mech}}}{\partial \boldsymbol{E}_{e_a}}\mathbf{F}_{\upsilon_a}^{-T}\mathbf{F}_C^{-T}, \tag{19}$$

where $\Psi_\infty^{\mathrm{mech}}$ and $\Psi_{\upsilon_\alpha}^{\mathrm{mech}}$ are the elastic contribution in a long-term equilibrium state and the elastic energy density stored in a Maxwell viscoelastic unit, α, respectively; $\mathbf{E}_M$ and $\mathbf{E}_{e_a}$ are the Green-Lagrange elastic strain tensors in the long-term equilibrium state and a Maxwell viscoelastic unit, α, respectively.

According to Bonet,[41] a linear relationship between the viscoelastic deformation rate and stress can be established to describe the viscoelastic behavior (Equation 20):

$$\mathbf{D}_{\upsilon_\alpha} = \frac{1}{2\eta_\alpha}\left(\sigma_\alpha - \frac{1}{3}\mathrm{tr}\,(\sigma_\alpha)\,\mathrm{I}\right) = \frac{1}{2\eta_\alpha}\,\tau_\alpha, \tag{20}$$

where $\mathbf{D}_{\upsilon_\alpha}$ is the rate of viscous deformation, expressed as $\mathbf{D}_{\upsilon_\alpha} = \dot{\mathbf{F}}_{\upsilon_a} \cdot \mathbf{F}_{\upsilon_a}^{-1}$[43]; tr(•) is the operator to calculate the trace of a matrix or tensor; $\tau_\alpha = \sigma_\alpha - \frac{1}{3}\mathrm{tr}(\sigma_\alpha)\mathrm{I}$ is the deviatoric part of the Cauchy stress; η_α is shear viscosity. For a generalized Maxwell viscoelastic model, the Maxwell viscosity, η_α, can be expressed in the form of $\eta_\alpha = A_\alpha G\tau_\alpha$, where A_α, τ_α, and G, are the weight factor and relaxation time associated with the Maxwell unit α, and shear modulus of glass, respectively. The governing equations of the ternary IOX glass model are listed in Table 1. The detailed derivation of the strain energy density and the entropy imbalance for the system is described in the Supporting Information Note 1.

2.3 | NN model for IOX

While it is expected that the proposed computational model can provide accurate predictions of the key indices of strengthening effect, such as SCS and the depth of the layer under compression (DOC), the parameters employed in the model are largely unknown prior; hence, substantial effort (i.e., many trials of simulations) is required to calibrate the model. In this work, a parametric calibration process is described based on detailed experimental work.[46] In implementation, such a calibration process must be conducted when the chemical composition of glass is changed, which could be very tedious. Therefore, we suggest an alternative way for the industry, that is, to train a surrogate model to predict SCS and DOC using experimental data, instead of knowing details of model parameters for the simulation. In this work, we suggest a back-propagation neural network (BPNN) to predict SCS and DOC under specific IOX conditions. The BPNN is trained using simulation results, that is, the BPNN is the surrogate model replacing the IOX computational model (Figure 3). The proposed BPNN predicts SCS and DOC

TABLE 1 Governing equations of the ternary IOX glass model.

Diffusion equation	$\frac{\partial \bar{c}_i}{\partial t} = D_i \nabla^2 \bar{c}_i - \frac{\mu_i \bar{c}_i (\nabla j_0 + \sum_i^{N-1}[(D_i - D_N)\nabla^2 \bar{c}_i])}{\sum_i^{N-1}[(\mu_i - \mu_N)\bar{c}_i] + \mu_N} + \left(\frac{\mu_i \bar{c}_i (\sum_i^{N-1}[(\mu_i - \mu_N)\nabla \bar{c}_i])}{\sum_i^{N-1}[(\mu_i - \mu_N)\bar{c}_i] + \mu_N} - \mu_i \nabla \bar{c}_i \right) \cdot \left(\frac{\sum_i^{N-1}[(D_i - D_N)\nabla \bar{c}_i]}{\sum_i^{N-1}[(\mu_i - \mu_N)\bar{c}_i] + \mu_N} + \nabla \varphi_{\text{apply}} \right)$
Poisson equation	$\nabla^2 \varphi_{\text{apply}} = 0$
Hydrostatic equations	$\text{div}\,(\det(\mathbf{F})^{-1}\mathbf{P}\mathbf{F}^{\mathrm{T}}) = 0$

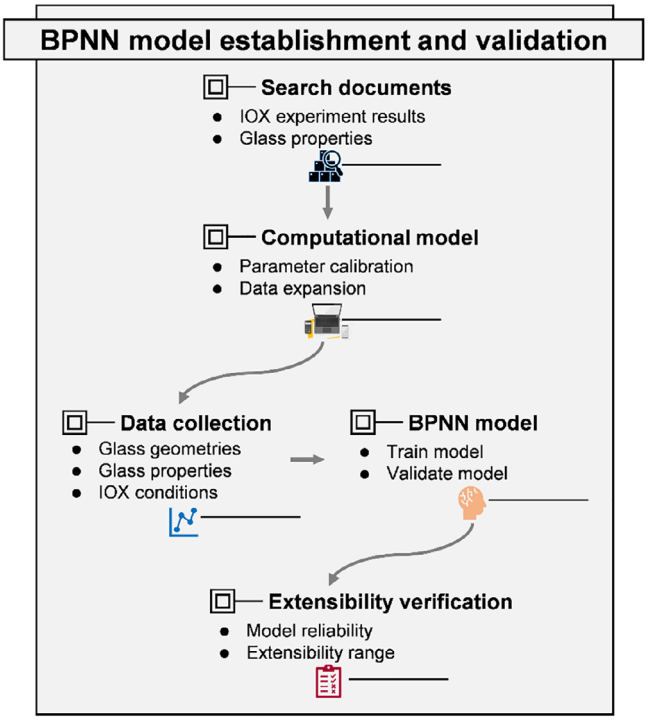

FIGURE 3 Schematics of BPNN model establishment. BPNN, back-propagation neural network.

based on the inputs of relaxation time, ion diffusivity, molten salt composition, glass thickness, and duration. Among them, relaxation time and ion diffusivity are functions of temperature; hence, these two parameters can be replaced by temperature when the diffusivity and relaxation time are unclear for a glass. It must be emphasized that glass thickness is also an important parameter because thinner glass tends to have larger lateral expansion which leads to a reduction in SCS and an increase in central tension. The discussion of the thickness effect can be found in the Supporting Information.

3 | NUMERICAL MODELS AND RESULTS

We then numerically study a ternary IOX process for strengthening a kind of lithium-containing glass (64.5% SiO_2-20.5% Al_2O_3-4.5%Li_2O-0.7%MgO-0.349% Na_2O-0.3% K_2O-2.2% TiO_2-7% ZrO_2 (all in wt%)), which is immersed in a molten salt mixture containing K^+ and Na^+. The parameters, after calibrated based on experimental results provided in,[46] are listed in Table 2. The COMSOL Multiphysics modeling software[45] is used to solve the above governing equations. The calibration of parameters is described below, followed by a discussion of the parametric effects. Finally, an NN model is proposed to summarize these effects and make predictions based on process parameters.

3.1 | Parameter calibration based on thick glass

Distributions of stress and exchanged ion concentrations in a lithium-containing glass after Li–Na–K ternary IOX were measured by Hödemann[46] using their optical system based on the bending of the optical path in an IOX-strengthened glass. Their samples were thick (3 mm) lithium-containing silicate glasses, strengthened at 480°C and for 1–16 h in molten salts containing 80 mol% KNO_3 and 20 mol% $NaNO_3$. We simulated their IOX process for 1–16 h and determined the parameters by comparing them with the experimental results provided in the study by Hödemann,[46] as shown in Figure 4. These set of parameters are to be used for further analysis based on the computational models.

Because Na^+ ions diffuse much faster than K^+ ions in the glass, the stress profile after ternary IOX exhibits a clear stepwise distribution along the depth, as shown in Figure 4A. The 4 h IOX results in an SCS of −0.769 GPa and a rapid decrease in the compressive stress with the increase in depth until it reaches a transition point. Beneath this point, the stress varies gently from compressive to tensile, which is owing to the Na–Li exchange that can reach a much deeper layer than the K–Na exchange. The transition (i.e., from steep to gentle change of stress) point is generally called the knee point (also known as the breaking point).[46] The distance from the glass surface to the knee point is defined as the depth of the knee point, denoted by DOL_{kp} (as shown in Figure 4B, DOL_{kp} = 25.5 μm after 4 h IOX), and the stress located at the knee point

TABLE 2 Parameters used in the simulation.

	Parameter	Value
Ideal gas constant	R	8.314 J mol^{-1} K^{-1}
Faraday constant	F	96 485 C mol^{-1}
Young's modulus of glass	E	65.1 GPa[47]
Poisson's ratio	ν	0.22[48]
Relaxation time	τ	$3.6 \times 10^6 - 3.6 \times 10^5$ s
Diffusion coefficient of Na^+ in glass	D_{Na^+}	$1.5 - 3.5 \times 10^{-13}$ m^2 s^{-1}
Diffusion coefficient of K^+ in glass	D_{K^+}	$4.0 - 8.0 \times 10^{-15}$ m^2 s^{-1}
Na–Li exchange volumetric strain	ε^{eg}_{Na-Li}	0.001 − 0.005
K–Na exchange volumetric strain	ε^{eg}_{K-Na}	0.01 − 0.014
Coefficient to scale the effect of stress on diffusivity	ξ	$0 - 1.5 \times 10^{-5}$ m^3 mol^{-1}
Interface diffusion rate of Na^+	$D^{I/F}_{Na^+,0}$	4.0×10^{-13} m^2 s^{-1}
Interface diffusion rate of K^+	$D^{I/F}_{K^+,0}$	16×10^{-12} m^2 s^{-1}

is denoted by σ_{kp}, ($\sigma_{kp} = -0.186$ GPa after 4 h IOX as shown in Figure 4A). In our numerical results, the total DOL experienced IOX is defined as the distance from the surface to the location where $\bar{c}_{Na^+} = 0.001$ as shown in Figure 4B. In a thick glass (i.e., glass thickness much larger than DOL), DOC is equal to DOL, which is 276 μm in Figure 4A.

Through simulations, the relation between DOL and the diffusion coefficient, D_{Na^+}, is summarized in Figure 4C. It shows that when D_{Na^+} is 2.5×10^{-13} m^2 s^{-1}, the numerical model rendered a DOL variation almost identical to the experimental measurement. Similarly, the diffusion coefficient of K^+ can be determined to be $D_{K^+} = 6.0 \times 10^{-15}$ m^2 s^{-1}, based on the relation between DOL_{kp} and D_{K^+} as shown in Figure 4D.

To determine the volumetric strains due to IOX, namely, ε^{eg}_{Na-Li} and ε^{eg}_{Na-Li}, we plot the distribution of in-plane stress, σ_{11} to compare with experimental results. Because σ_{kp} is formed mainly due to the Na–Li exchange, the relation between σ_{kp} and ε^{eg}_{Na-Li}, as shown in Figure 4E, can lead to the determination of ε^{eg}_{Na-Li}. Figure 4E shows that if $\varepsilon^{eg}_{Na-Li} = 0.002$, the predicted stress at the knee point can agree with the experimental measurement. The SCS, σ_s, is induced by both Na–Li and K–Na exchanges. Thus, after determining diffusivities and ε^{eg}_{Na-Li}, we conduct further simulations to make the relation between σ_s and ε^{eg}_{Na-Li} explicit, as shown in Figure 4F. We determined that $\varepsilon^{eg}_{Na-Li} = 0.012$, which leads to the agreement with the experimental results of 1 and 8 h. It is noted that experimental results of 4 and 16 h do not follow the trend (i.e., SCS increases with IOX duration). This could be caused by the competition of stress relation and the stuffing effect of increasing K^+ concentrations. In the simulation, to calibrate parameters without other impact factors, stress relaxation is not considered, so SCS increases with the exchanged number of ions. In actual cases, the effect of stress relaxation is slight during the first four hours. However, as time goes by, the influence of stress relaxation outweighs the stuffing effect, leading to a decreased SCS with time.

To further investigate the influence of stress relaxation, we employ a Maxwell viscoelastic model to simulate this phenomenon,[47,48] and set a characteristic relaxation time, τ, ranging from 9×10^5 to 3.6×10^6 s. The results are illustrated in Figure 5. Notably, when $\tau = 1.8 \times 10^6$ s, the simulation results align closely with the experimental measurements. Discrepancies remain when comparing the 1 and 4 h simulation results with the experimental data. This difference is likely attributed to additional relaxation mechanisms. It is worth highlighting that two types of stress relaxation occur in an ion-exchanged glass, that is, slow (α) shear viscosity-related relaxation and fast (β) structural relaxation.[49] While the present model and several theoretical investigations of IOX[49–52] focus only on α stress relaxation, β relaxation also plays a crucial role in the ion exchange process. Donal et al.[53] and Schaut[54] found that the surface compressive stresses gradually decreased to zero with the increase in IOX time and that the surface stresses could eventually be tensile.[1] Varshneya[48,49] proposed the volumetric relaxation mechanisms (such as densification or collapse of silica skeletons under high pressure) and developed a viscoelastic model consisting of a series of Maxwell and Voigt-Kelvin elements to describe the complex relaxation behavior. However, we do not adopt Varshneya's model due to the challenges in parameterizing the complicated viscoelastic model for the specific glass studied experimentally by Hödemann et al.[46] Additionally, inherent inaccuracies in measurements, such as those arising from the compensation algorithm employed by Hödemann et al.,[46] may also contribute to the

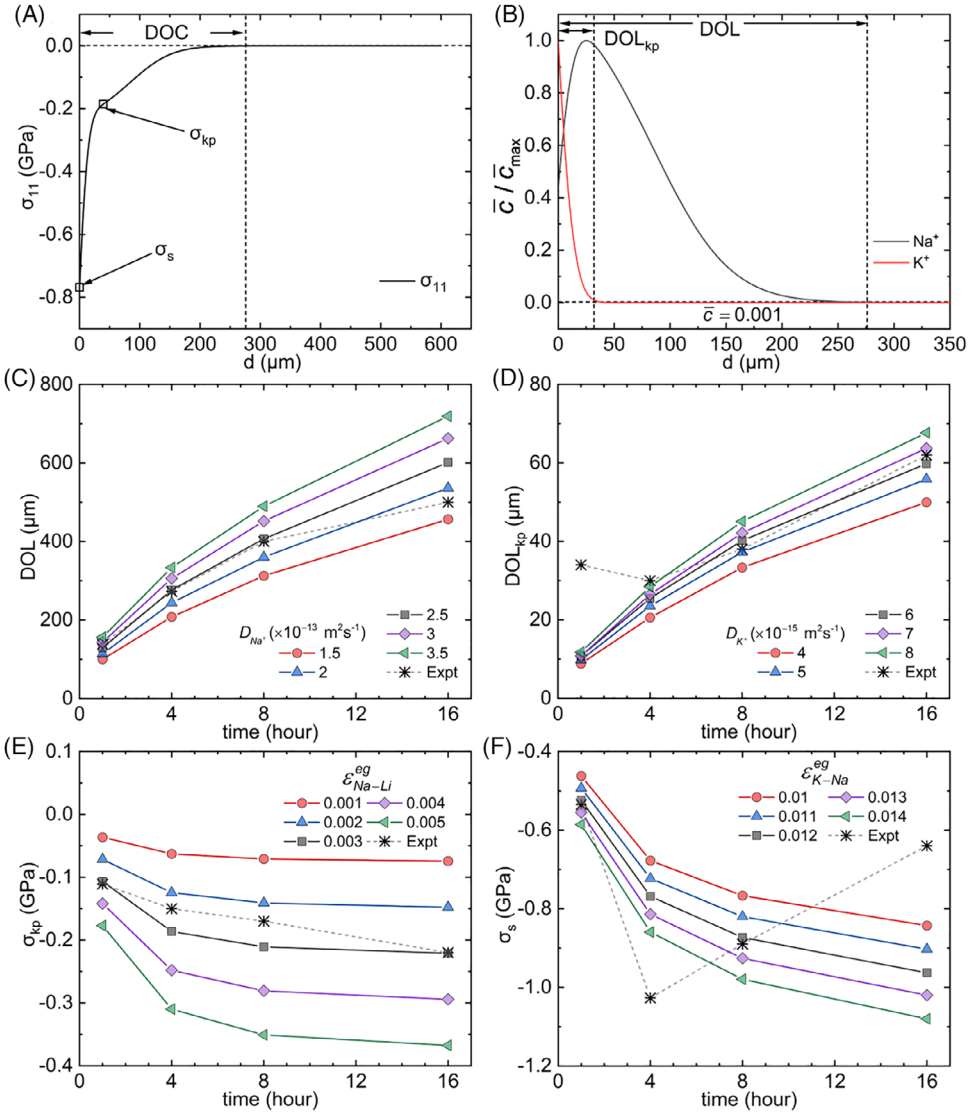

FIGURE 4 Simulation versus experimental[46] results for parameter calibration. (A, B) Distribution of stress and dimensionless relative concentration of Na^+ and K^+ after 4 h IOX to exemplify the simulation results and determinations of key measurements. (C–F) Variations of DOL, DOL_{kp}, σ_{kp}, and SCS with IOX duration, which are used to determine the key parameters D_{Na^+}, D_{K^+}, ε^{eg}_{Na-Li}, and ε^{eg}_{K-Na}, respectively. IOX, ion exchange; SCS, surface compressive stress.

discrepancies observed between experimental and simulation results.

To recapitulate, the experimentally calibrated parameters used in this work are: $D_{Na^+} = 2.5 \times 10^{-13}$ m^2s^{-1}, $D_{K^+} = 6.0 \times 10^{-15}$ m^2s^{-1}, $\varepsilon^{eg}_{Na-Li} = 0.002$, $\varepsilon^{eg}_{K-Na} = 0.012$. These parameters are determined by only using experimental results of σ_s, σ_{kp}, DOL, and DOL_{kp}, which are always measured after IOX experiments even in the glass industry for quality assurance. Hence, the above calibration process can be directly implemented using industrial data.

With the calibrated parameters, the further comparisons between simulation and experimental results are shown in Figure 6A–D, where the distributions of sodium concentration $\bar{c}_{Na^+}/\bar{c}_{Na^+,\,max}$ and in-plane residual stress σ_{11} are shown for the cases of K–Na–Li IOX for 1, 4, 8, and 16 h. In general, the simulation results agree well with experimental results, but the sodium concentration profile becomes less consistent with experimental results in the cases with IOX durations longer than one hour. Take the 4 h result (Figure 6D) as an example, the experimentally measured sodium concentration decreases almost linearly after a peak (where the knee point is located), while the simulation result shows an exponential and faster decrease. It can be inferred that the diffusion in the low-sodium-concentration zone should be speedier than the simulation based on constant diffusivity, resulting in a higher sodium concentration in experiments.

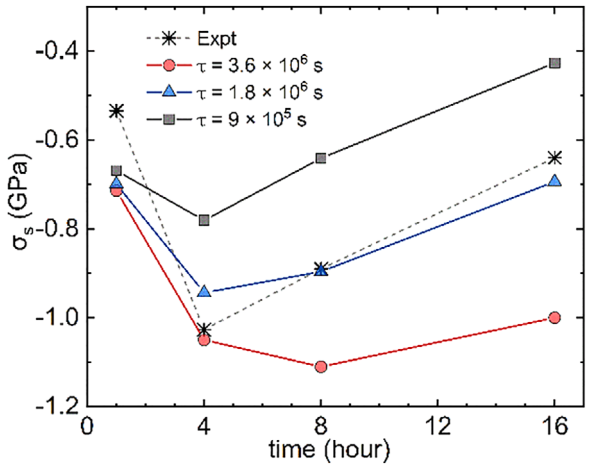

FIGURE 5 Variations of SCS with IOX duration of different relaxation time. IOX, ion exchange; SCS, surface compressive stress.

The discrepancy in sodium concentration indicates that the diffusivity of sodium, D_{Na^+}, could be concentration-dependent.[55–57] To address this, an exponential relation is proposed to relate the sodium diffusivity with sodium concentration (cf. also[58–63]): $D_{Na^+} = D^0_{Na^+} \cdot e^{-3.209\bar{c}}$, where $D^0_{Na^+}$ denotes the initial sodium diffusivity when the concentration of Na^+ is zero. With this modification, the simulation results of Na^+ concentration can agree well with experimental results, as shown in Figure 6A–D. It is noted that similar phenomena have been observed in other materials.[60–62] Hristov[60] proposed that this might be attributed to structure relaxation, described as a delayed response of the structure to the local dilations of ion accumulations during diffusion. Some theories focus on an interaction among neighboring cations, in which mixed pairs are assumed to be more energetically stable than pairs of cations of the same species (i.e., mixed effect[58]). The energy barrier that ion diffusion should overcome among mixed pairs is higher, resulting in the slower diffusion of Na^+ in the area with higher sodium concentration.

Since the depth of the knee point, DOL_{kp}, the total depth of exchanged layer, DOL, the stress of the knee point, σ_{kp}, and the surface stress, σ_s, are the four important indexes for the evaluation of strengthening effect, their variations with IOX treatment time are summarized in Figure 6E,F. Figure 6E shows approximately a square-root-time dependence of DOL_{kp} and DOL, which is the typical result of diffusion. In Figure 6F, σ_{kp} and σ_s increases with increasing time, this is because the exchanged amount of sodium and potassium increases over time. It is noted that after 12 h σ_s remains relatively constant, indicating that the K–Na exchange has reached its maximum.

3.2 | Effect of molten salt composition

In IOX treatments, the composition of molten salt (i.e., the concentration ratio of K^+ and Na^+) is an important process parameter to optimize the strength of glass, but the study of the effect is scarce in the literature. To investigate the effect of salt composition, we assumed finite rates of cations crossing the interface from the molten salt to glass. In numerical implementation, we assumed a finite wide of the interface and diffusion equations within the interface. The interface diffusion rates $D^{I/F}_{Na^+}$ and $D^{I/F}_{K^+}$ are then the diffusion coefficients of the corresponding equations governing the interface crossing of cations Na^+ and K^+ from molten salt to glass, respectively. In this section, using the calibrated parameters, we adjust the ratio of Na^+ and K^+ concentrations in a molten salt by controlling the interface diffusion rates $D^{I/F}_{Na^+}$ and $D^{I/F}_{K^+}$, for sodium and potassium ions, respectively. In other words, we presumed that the concentrations of cations in the molten salt are much larger than those in glass, and the rate-limiting factor is the interfacial transport coefficients, and we further assume that $D^{I/F}_{Na^+} : D^{I/F}_{K^+} = \bar{c}_0^{Na^+} : \bar{c}_0^{K^+}$. Figure 7A,B show the distribution of σ_{11}, $\bar{c}_{Na^+}$ and $\bar{c}_{K^+}$ after 4 h strengthening along the depth of glass with a molten salt ratio $\bar{c}_0^{Na^+} : \bar{c}_0^{K^+} = 1{:}0.25 \sim 1{:}4$, with fixing $D^{I/F}_{Na^+} = D^{I/F}_{Na^+,0}$.

It is apparent that the exchanged K^+ increases with increasing $\bar{c}_0^{K^+}$, resulting in an increase in SCS, as shown in Figure 7A. Even when $\bar{c}_0^{K^+}$ is greater than $\bar{c}_0^{Na^+}$, due to the limited diffusivity of K^+, K^+ cannot completely replace Na^+, K–Na IOX is still dominated by the concentration of K^+ in the salt.

Figure 7C,D show the distribution of σ_{11}, $\bar{c}_{Na^+}$, and $\bar{c}_{K^+}$ after 4 h strengthening along the depth of glass with molten salt ratio, $\bar{c}_0^{Na^+} : \bar{c}_0^{K^+} = 0.25{:}1 \sim 4{:}1$, that is, we fix $D^{I/F}_{K^+} = D^{I/F}_{K^+,0}$ and change the flux of Na^+. The exchanged Na^+ increases with the increase in $\bar{c}_0^{Na^+}$, which results in a larger DOL and an increase in both σ_s and σ_{kp} as shown in Figure 7C. Since the exchanged Na^+ is bounded by the concentration of Li^+ in the original glass, when $\bar{c}_0^{Na^+} : \bar{c}_0^{K^+}$ is larger than 0.5:1, increasing the ratio leads to almost no difference in SCS, indicating that Na^+ is nearly completely replaced by K^+, such a phenomenon has also been observed by Varshneya et al.[64]

The evolutions of DOL_{kp}, DOL, σ_{kp}, and σ_s with the different molten salt compositions are summarized in Figure 8. If the fluxes of Na^+ and IOX duration are fixed, DOL will not change, but DOL_{kp} σ_{kp}, and σ_s increase with $\bar{c}_0^{K^+}$ or the interfacial flux of K^+, as shown in Figure 8A,B. Similarly, if $\bar{c}_0^{K^+}$ or the interfacial flux of K^+ is fixed, DOL

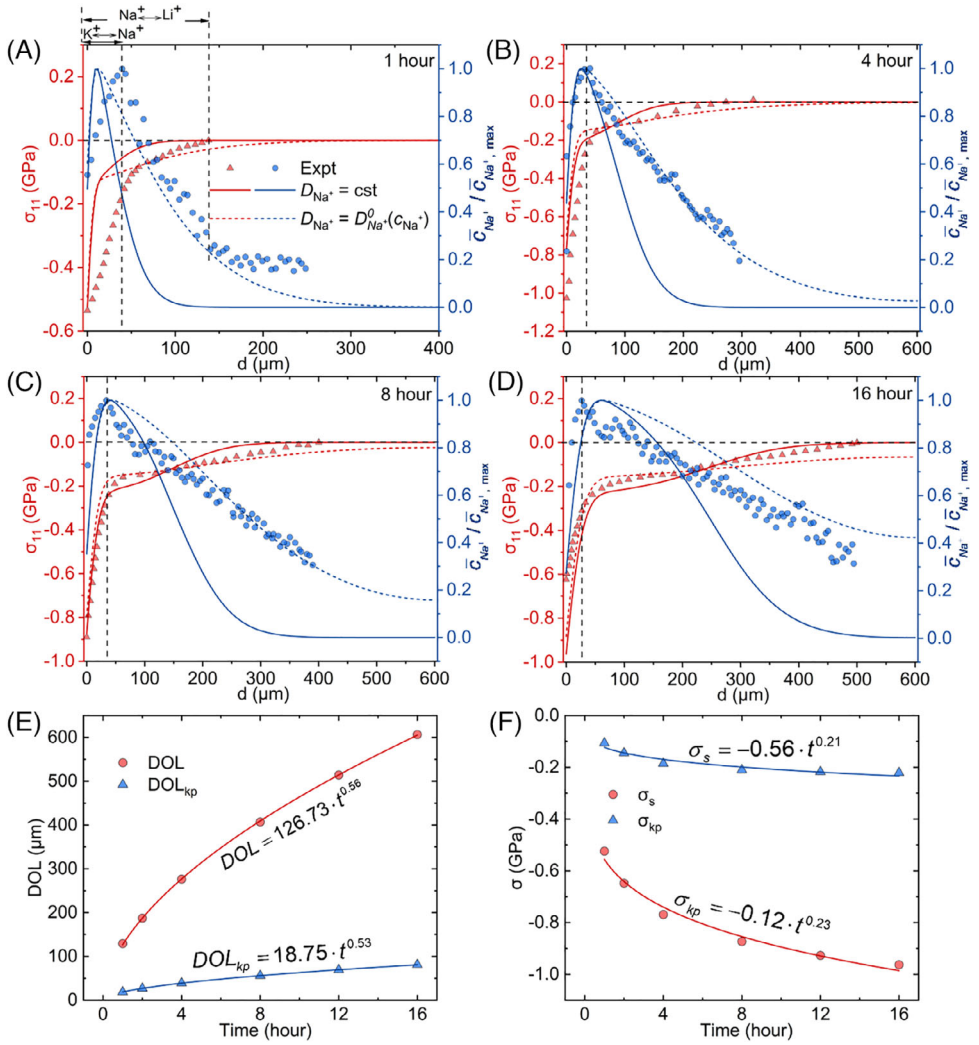

FIGURE 6 Distribution of dimensionless relative concentration of Na^+, $\bar{c}_{Na^+}/\bar{c}_{Na^+,\,max}$(blue line), and in-plane stress, σ_{11}(red line), along the glass thickness direction after K–Na–Li IOX with constant diffusivity(solid line) and concentration-dependent diffusivity(dashed line) after different IOX durations ((A–D) for 1, 4, 8, and 16 h, respectively); (E) the power law (square root of time) between DOL, DOL_{kp}, and IOX duration (F) the power law between σ_{kp}, σ_s, and IOX duration. DOL, depth of layer; IOX, ion exchange.

increases with $\bar{c}_0^{Na^+}$, as shown in Figure 8C, but the residual stresses do not change much when $\bar{c}_0^{Na^+}$:$\bar{c}_0^{K^+}$ is larger than 0.5, as shown in Figure 8D.

3.3 | NN model-based IOX prediction

In this section, a BPNN is described to predict SCS and DOC based on the computational model in previous sections. As shown in Figure 9, the proposed BPNN model comprises ten layers, including an input layer, an output layer, and eight hidden layers. The number of neurons in each hidden layer is 15, 15, 15, 12, 12, 12, 10, and 4. The sigmoid function is selected as the activation function. Due to the high training rate of the Levenberg–Marquardt algorithm, it is utilized in the BPNN training (i.e., to update weights and biases).

Based on the results obtained from the computational model, 1028 sets of IOX data were employed to train and test the BPNN's prediction performance with a ratio of 7:3. The detailed data used is listed in Table 3. Figure 10 exhibits the comparisons between the prediction results of training and testing data. Standard deviation (SD) and R square value (R^2) were adopted to evaluate the prediction accuracy and were commonly used to assess the prediction performance of a machining learning model. As shown in Figure 10A,B, both SCS and DOC are well predicted for the training group. Referring to the numerical ranges of SCS and DOC, the SD values were small with values of 0.0261 and 0.0179, respectively. R^2 values of SCS and DOC of the training group were both close

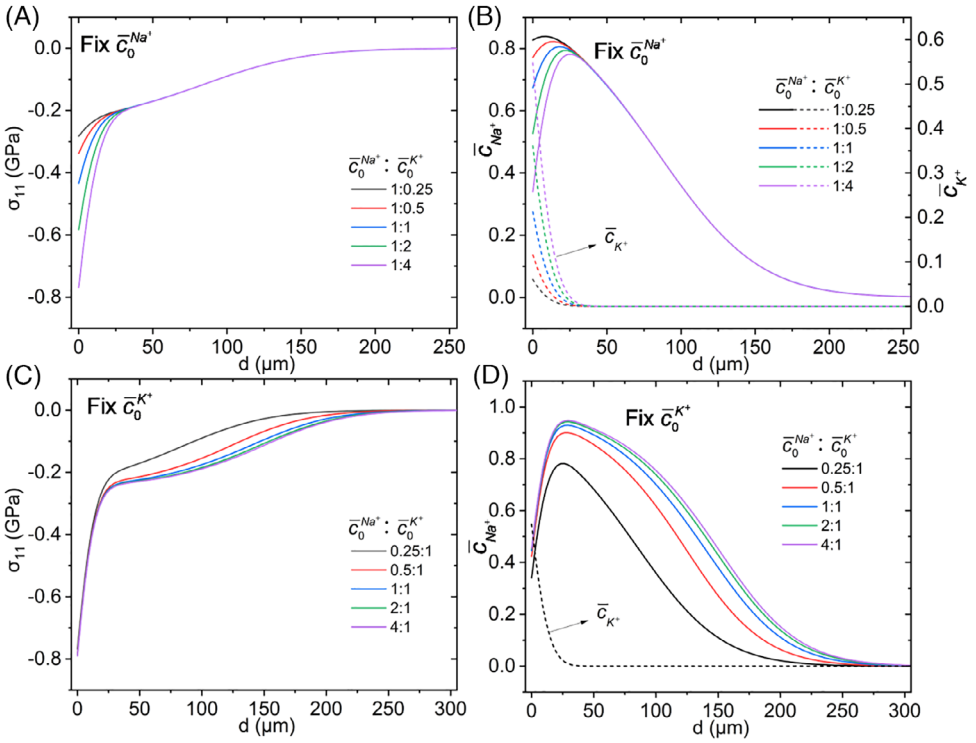

FIGURE 7 Distribution of in-plane stress σ_{11}(A), $\bar{c}_{Na^+}$(B left axis), and $\bar{c}_{K^+}$(B right axis) along the glass thickness direction for different ratios of $\bar{c}_0^{Na^+}$ and $\bar{c}_0^{K^+}$, when fixing $\bar{c}_0^{Na^+}$ and 4 h of strengthening; Distribution of in-plane stress σ_{11}(B), $\bar{c}_{Na^+}$(D), and $\bar{c}_{K^+}$(D) along the glass thickness direction for different ratios of $\bar{c}_0^{Na^+}$ and $\bar{c}_0^{K^+}$, when fixing $\bar{c}_0^{K^+}$ and 4 h of strengthening.

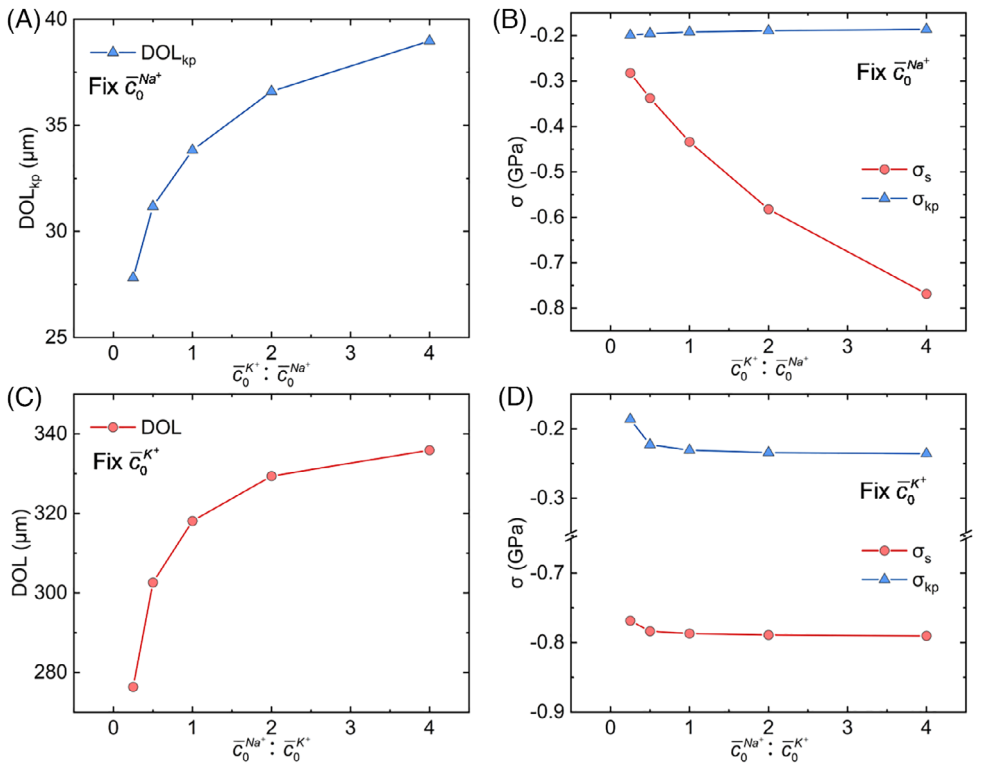

FIGURE 8 (A) Variation of DOL_{kp} with $\bar{c}_0^{K^+}$: $\bar{c}_0^{Na^+}$; (B) variation of σ_{kp}、σ_s with $\bar{c}_0^{K^+}$: $\bar{c}_0^{Na^+}$; (C) variation of DOL with $\bar{c}_0^{Na^+}$: $\bar{c}_0^{K^+}$; (D) variation of σ_{kp}、σ_s with $\bar{c}_0^{Na^+}$: $\bar{c}_0^{K^+}$. DOL, depth of layer.

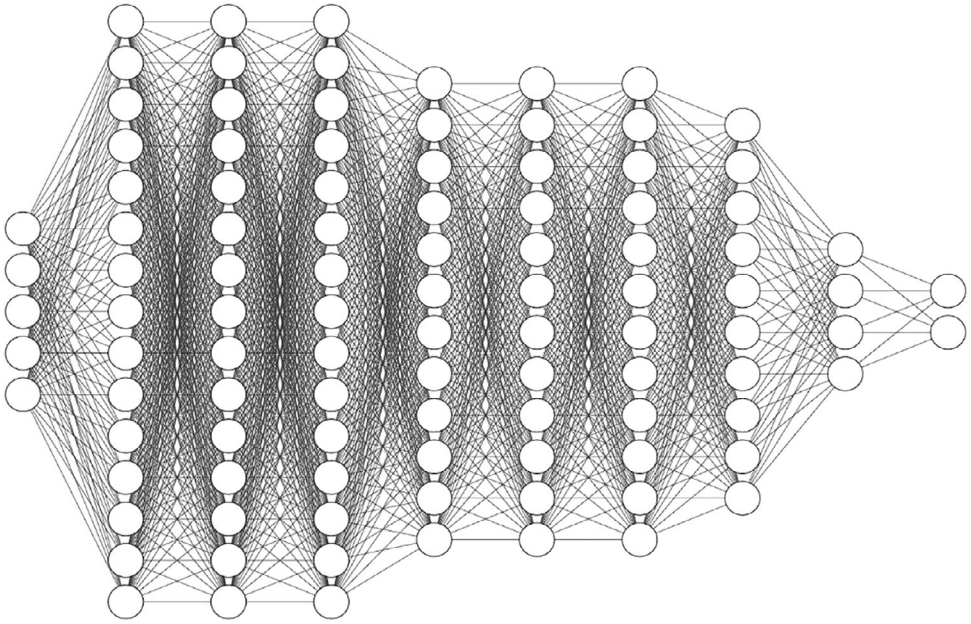

FIGURE 9 Structure of BPNN model. BPNN, back-propagation neural network.

TABLE 3 Data used in the BNPP model.

	Training	Testing	Validation I	Validation II
Number of cases used	720	308	48	72
Temperature (°C)	460–500	460–500	500	460
Relaxation time ($\times 10^{-8}$ s^{-1})	4.48–12.32	4.48–12.32	12.32	4.48
Na^+ diffusivity ($\times 10^{-13}$ m^2 s^{-1})	2.2–2.62	2.2–2.62	2.62	2.2
Molten salt ratio $\bar{c}_0^{Na^+}$:$\bar{c}_0^{K^+}$	0.05–2	0.05–2	0.43, 2	0.005
Glass thickness (μm)	100–600	100–600	600	600
Strengthening time (h)	1–24	1–24	1–24	1–24

to 1, indicating that the BPNN model could provide accurate predictions. For the prediction of data in the testing group, SD values of SCS and DOC were 0.0343 and 2.1606, while R^2 values were 0.97757 and 0.99504, respectively. The results shown in Figure 10 demonstrated that the BPNN model has been adequately trained to predict IOX results.

The generality of the BPNN model can be demonstrated by verifying the accuracy in predicting cases that have not been previously trained. Two validations were conducted in this section, one (Validation I) employed inputs within the training range but recombined, and the other (Validation II) employed inputs out of the training range with a Na–K ratio in molten salt ten times smaller than the lower bound of the training set. Figure 11 exhibits the prediction results of these two validations. The prediction results of recombined cases are accurate with SD and R^2 similar to those shown in Figure 10A,B. In the training group, the range of molten salt ratio $\bar{c}_0^{Na^+}$: $\bar{c}_0^{K^+}$ is 0.05:1 ~ 1:2. The IOX results with $\bar{c}_0^{Na^+}$: $\bar{c}_0^{K^+}$ = 0.005:1 are predicted in Validation II and compared with the results of the computational model. As shown in Figure 11C,D, the predictions of SCS and DOC are accurate with low SDs and R^2s above 0.8. Hence, this BPNN model shows a good ability to do validation and extrapolation.

4 | CONCLUSION

This research proposed a mechanochemical strengthening model for ternary IOX, characterized by a constitutive relation formulated within a large-strain framework and incorporating generalized Maxwell viscoelasticity. The model integrates critical factors such as stress-dependent

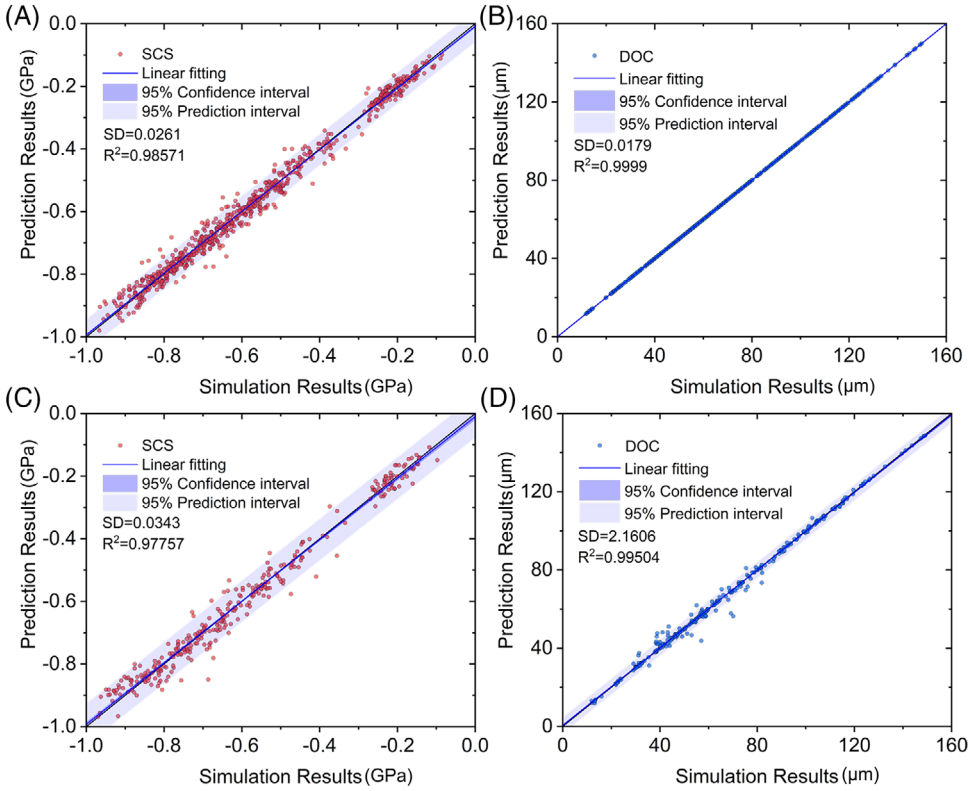

FIGURE 10 Prediction results of BPNN model: (A) training group of SCS, (B) training group of DOC, (C) testing group of SCS, (D) testing group of DOC. BPNN, back-propagation neural network. DOL, depth of layer; SCS, surface compressive stress.

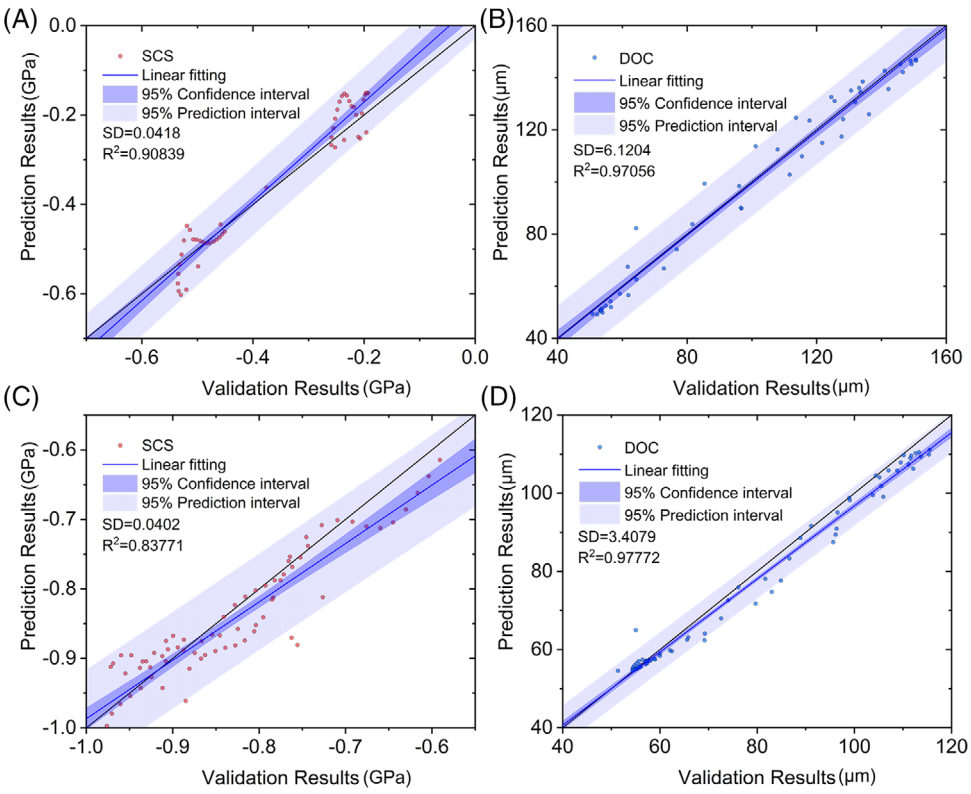

FIGURE 11 Prediction results of BPNN model: (A) SCS results of Validation I, (B) DOC results of Validation I, (C) SCS results of Validation II, (D) DOC results of Validation II. BPNN, back-propagation neural network; DOL, depth of layer; SCS, surface compressive stress

diffusivity, mass conservation, electroneutrality, and the Nernst–Plank equation, leading to the derivation of governing equations applicable to ternary IOX. Utilizing experimental data from the study by Hödemann et al.,[46] the model parameters were systematically determined, and the influence of molten salt composition was then investigated. It was indicated that for the specific glass composition analyzed, an optimal Na–K ratio of 0.5:1 in the molten salt was essential for maximizing SCS. Furthermore, increasing the Na^+ content to make the Na–K ratio beyond this optimal value would not yield additional improvements in SCS.

Additionally, a BPNN model was developed to predict SCS and DOC based on input parameters related to the IOX process and glass geometry. The neural network, comprising eight hidden layers and 95 neurons, demonstrates robust predictive capabilities, suggesting its potential as a surrogate model to substitute conventional finite element simulations.

ACKNOWLEDGMENTS

The authors acknowledge support from the Hong Kong GRF (grant number 15210622), industry (HKPolyU project ID: P0039303), and research and development funding from CNERC and the Hetao Shenzhen-Hong Kong Science and Technology Innovation Cooperation Zone Project (no. HTHZQSWS-KCCYB-2023042). Additionally, the authors thank the Natural Science Foundation of Guangdong Province (2022A1515011891, 2024A1515011127), the Natural Science Basic Research Plan in Shaanxi Province (grant number 2022JQ-019), and the "Young Top Talents" program in the Pearl River Talent Project of Guangdong Province (2021QN02L344).

CONFLICT OF INTEREST STATEMENT

The authors declare no conflict of interest.

ORCID

Junju Xu https://orcid.org/0009-0009-9217-7519
Haihui Ruan https://orcid.org/0000-0002-9233-8820

REFERENCES

1. Macrelli G, Varshneya AK, Mauro JC. Simulation of glass network evolution during chemical strengthening: resolution of the subsurface compression maximum anomaly. J Non-Cryst Solids. 2019;522:119457.
2. Wang M, Jiang L, Li X, Liu J, Li J, Yan Y. Structure and mechanical response of chemically strengthened aluminosilicate glass under different post-annealing conditions. J. Non-Cryst Solids. 2021;554:120620.
3. Karlsson S, Jonson B, Stålhandske C. The technology of chemical glass strengthening-a review. Glass Technology. 2010;51(2):41–54.
4. Varshneya AK. Chemical strengthening of glass: lessons learned and yet to be learned. Int J Appl Glass Sci. 2010, 1(2).
5. Kistler SS. Stresses in glass produced by nonuniform exchange of monovalent ions. J Am Ceram Soc. 1962;45(2):59–68.
6. Acloque P. Measurement of the mechanical strength of glass after reinforcement. Comptes Rendus. 1962:687–704.
7. Guo Y, Liu C, Wang J, Ruan J, Xie J, Han J, et al. Effects of alkali oxides and ion-exchange on the structure of zinc-alumino-silicate glasses and glass-ceramics. J Eur Ceram Soc. 2022;42(2):576–88.
8. Jiang Q, Yan J, Wang L, Chen C, Smith AT, Sun L, et al. Chemical strengthening of Li^+-containing phosphosilicate glass via a two-step ion-exchange process. J Aust Ceram Soc. 2021;57(4):1285–90.
9. Liu C, Ren Q, Huang Q, Liu T, Zhang Q, Lu A. Study of high-alumina-silicon glass structure and performance modified by Li_2O replacing Na_2O. J Non-Cryst Solids. 2021;572:121115.
10. Zou J, Zhao F, Chen RT. Two-step K+–Na+ and Ag+–Na+ ion-exchanged glass waveguides for C-band applications. Appl Optics. 2002;41(36):7620–26.
11. Zhou Z, Duan X. Integrated waveguide splitter fabricated by Cs+–Na+ ion-exchange. Optics Commun. 2006;266(1):129–31.
12. Jiang L, Guo X, Li X, Li L, Zhang G, Yan Y. Different K^+–Na^+ inter-diffusion kinetics between the air side and tin side of an ion-exchanged float aluminosilicate glass. Appl Surf Sci. 2013;265:889–94.
13. Varshneya AK, Spinelli IM. High-strength, large-case-depth chemically strengthened lithium aluminosilicate glass. American Ceramic Society Bulletin 2009;88(5):27–33.
14. Varshneya AK. Kinetics of ion exchange in glasses. J Non-Cryst Solids. 1975;19:355–65
15. Mallick KK, Holland D. Strengthening of container glasses by ion-exchange dip coating. J Non-Cryst Solids. 2005;351(30-32):2524–36.
16. Spirkova J, Tresnakova-Nebolova P, Mika M. Optical waveguides fabricated by transition element ions exchange in some commercial and special optical glasses. Optical Mater. 2004;25(2):101–7.
17. Tagantsev DK, Karapetyan GO, Lipovskii AA, Loboda VV. Formation of thick glass-ceramics films by ion-exchange. J Eur Ceram Soc. 2001;21(10-11):2015–18.
18. Calahoo C, Zwanziger JW, Butler IS. Mechanical–structural investigation of ion-exchanged lithium silicate glass using micro-Raman spectroscopy. J Phys Chem C. 2016;120(13):7213–32.
19. Hödemann S, Valdmann A, Anton J, Murata T. Gradient scattered light method for non-destructive stress profile determination in chemically strengthened glass. J Mater Sci. 2016;51:5962–78.
20. Kuwata N, Lu X, Miyazaki T, Iwai Y, Tanabe T, Kawamura J. Lithium diffusion coefficient in amorphous lithium phosphate thin films measured by secondary ion mass spectroscopy with isotope exchange methods. Solid State Ionics. 2016;294:59–66.
21. Andrews RC, Roussev RV, Schneider VM. Methods of characterizing ion-exchanged chemically strengthened glasses containing lithium: U.S. Patent 9,897,574[P]. 2018-2-20.
22. Aaldenberg EM, Lezzi PJ, Seaman JH, Blanchet TA, Tomozawa M. Ion-exchanged lithium aluminosilicate glass: strength and dynamic fatigue. J Am Ceram Soc. 2016;99(8):2645–54.

23. Kishii T. Surface stress meters utilising the optical waveguide effect of chemically tempered glasses. Optics Lasers Eng. 1983;4(1):25–38.
24. Gonella F, Cattaruzza E, Quaranta A, et al. Diffusion behavior of transition metals in field-assisted ion-exchanged glasses. Solid State Ionics. 2006;177(35-36): 3151–55.
25. Cattaruzza E, Battaglin G, Gonella F, et al. Chromium doping of silicate glasses by field-assisted solid-state ion exchange. J Non-Cryst Solids. 2011;357(8-9):1846–50.
26. Cattaruzza E, Gonella F, Peruzzo G, et al. Field-assisted ion diffusion in dielectric matrices: Er^{3+} in silicate glass. Mater Sci Eng: B. 2008;146(1-3):163–66.
27. Inman, JM; Houde-Walter, S; McIntyre, BL; Liao, ZM; Parker, RS, Simmons, V. Chemical structure and the mixed mobile ion effect in silver-for-sodium ion exchange in silicate glass. J Non-Cryst Solids. 1996;194, 85–92.
28. Lupascu, A; Kevorkian, A; Bondet, T; Saint-André, F; Persegol, D; Levy, M. Modeling ion exchange in glass with concentration dependent diffusion coefficients and mobilities. Opt Eng. 1996;35, 1603–10.
29. Lezzi, P; Tomozawa, M. Enthalpy of mixing of mixed alkali glasses. J Non-Cryst Solids. 2010;356, 1439–46.
30. Lezzi, P; Tomozawa, M. Effect of alumina on enthalpy of mixing of mixed alkali silicate glasses. J Non-Cryst Solids. 2011;357, 2086–92.
31. Macrelli G, Mauro JC, Varshneya AK. Coupling of diffusion and chemical stress: the case of ion exchange in glass. J Am Ceram Soc. 2021;104(11):5599–613.
32. Weber N, Goldstein M. Stress-induced migration and partial molar volume of sodium ions in glass. J Chem Phys. 1964;41(9):2898–901.
33. Charles RJ. Structural state and diffusion in a silicate glass. J Am Ceram Soc. 1962;45(3):105–13.
34. Varshneya AK, DUMAIS GA. Influence of externally applied stresses on kinetics of ion exchange in glass. J Am Ceram Soc. 1985, 68(7):C–165–C–166.
35. Lin C, Wang J, Hung K, Wong EYC, Ruan H. Modeling of ion exchange in glass considering large viscoelastic deformation and mechano–electrochemical coupling. J Am Ceram Soc. 2022;105(8):5190–202.
36. Liu H, Fu Z, Yang K, et al. Machine learning for glass science and engineering: a review. J Non-Cryst Solids. 2021;557: 119419.
37. Onbaşlı MC, Tandia A, Mauro JC. Mechanical and compositional design of high-strength Corning Gorilla® glass. Handbook of materials modeling: applications: current and emerging materials, 2020:1997–2019.
38. Cassar DR. ViscNet: neural network for predicting the fragility index and the temperature-dependency of viscosity. Acta materialia. 2021;206:116602.
39. Krishnan NMA, Mangalathu S, Smedskjaer MM, et al. Predicting the dissolution kinetics of silicate glasses using machine learning. J Non-Cryst Solids. 2018;487:37–45.
40. Aaldenberg EM, Lezzi PJ, Seaman JH, et al. Ion-exchanged lithium aluminosilicate glass: strength and dynamic fatigue. J Am Ceram Soc. 2016, 99(8):2645–54.
41. Olmsted DL, Phillips R, Curtin WA. Modelling diffusion in crystals under high internal stress gradients. Model. Simul. Mater. Sci. Eng.. 2004, 12(5):781.
42. Haftbaradaran H, Song J, Curtin WA, Gao H. Continuum and atomistic models of strongly coupled diffusion, stress, and solute concentration. J Power Sources. 2011, 196(1):361–70.
43. de Souza Neto EA, Peric D, Owen DRJ. Computational methods for plasticity: theory and applications[M]. John Wiley & Sons, 2011.
44. Bonet J. Large strain viscoelastic constitutive models. Int J Solids Struct. 2001, 38(17):2953–68.
45. COMSOL Multiphysics Users' Guide. Available from http://www.comsol.com/
46. Hödemann S, Valdmann A, Paemurru M, et al. Measurement of stress build-up of ion exchange strengthened lithium aluminosilicate glass. J Am Ceram Soc. 2020; 103:2407–20.
47. Varshneya AK. Fundamentals of inorganic glasses, 2nd ed. Society of Glass Technology, UK, 2006 (pp. 289 ff).
48. Varshneya AK. Mechanical model to simulate buildup and relaxation of stress during glass chemical strengthening. J Non-Cryst Solids. 2016;433:28–30.
49. Varshneya AK, Olson GA, Kreski PK, Gupta PK. Buildup and relaxation of stress in chemically strengthened glass. J Non-Cryst Solids. 2015;427:91–97.
50. Sane AY, Cooper AR. Stress buildup and relaxation during ion exchange strengthening of glass. J Am Ceram Soc. 1987;70(2):86–89.
51. Seaman JH, Lezzi PJ, Blanchet TA, Tomozawa M. Degradation of ion-exchange strengthened glasses due to surface stress relaxation. J Non-Cryst Solids. 2014;403:113–23.
52. Sun H, Dugnani R. Precise residual stress profile in ion-exchanged silicate glass by modified contour method. J Eur Ceramic Soc. 2021;41(7):4355–68.
53. Schaut R. Investigation of Anomalous Tensile Stress Generation with Prolonged Ion Exchange. Alfred University. B.Sc. Thesis, TP2 N3 2002 SchR. 2002
54. Donald IW, Hill MJC. Preparation and mechanical behaviour of some chemically strengthened lithium magnesium aluminosilicate glasses. J Mater Sci. 1988;23(8):2797–809.
55. Doremus RH. Exchange and diffusion of ions in glass. J Phys Chem. 1964;68(8):2212–18.
56. Varshneya AK, Milberg ME. Ion exchange in sodium borosilicate glasses. J Am Ceram Soc. 1974;57(4):165–69.
57. Doremus RH. Mixed-alkali effect and interdiffusion of Na and K ions in glass. J Am Ceram Soc. 1974;57(11):478–80.
58. Gomez S, Morena R, Noni DM, Price JJ, Sick SJ. Scratch resistant glass and method of making. US9670088B2, 2017.
59. Dugnani R. Closed-form solution to the residual stresses in ion-exchanged silicate glass including concentration-dependent material properties. J Non-Cryst Solids. 2020;536:120012.
60. Hristov J. On the nonlinear diffusion with exponential concentration-dependent diffusivity: integral-balance solutions and analyzes. Chapter 3. 2020:55–92.
61. Hedenqvist MS, Ritums JE, Condé-Brana M, et al. Sorption and desorption of tetrachloroethylene in fluoropolymers: effects of the chemical structure and crystallinity. J Appl Polymer Sci. 2003;87(9):1474–83.
62. Doroudiani S, Chaffey CE, Kortschot MT. Sorption and diffusion of carbon dioxide in wood-fiber/polystyrene composites. J Polymer Sci Part B: Polymer Phys. 2002;40(8):723–35.
63. Prieto-Blanco X, Montero-Orille C. Theoretical modelling of ion exchange processes in glass: advances and challenges. Appl Sci. 2021;11(11):5070.

64. Varshneya AK. Chemically strengthened lithium aluminosilicate glass having high strength effective to resist fracture upon flexing. US Patent. US8304078B2. 2012.

SUPPORTING INFORMATION

Additional supporting information can be found online in the Supporting Information section at the end of this article.

How to cite this article: Xu J, Zhang Y, Zhang Y, Lin C, Gao Z, Ruan H. Modeling of ternary ion exchange and stress evolution in lithium-containing glass. J Am Ceram Soc. 2025;108:e20217. https://doi.org/10.1111/jace.20217